A semiconducting polymer nano-prodrug for hypoxia-activated synergetic photodynamic cancer therapy

Cui, Dong; Huang, Jiaguo; Zhen, Xu; Li, Jingchao; Jiang, Yuyan; Pu, Kanyi

2019

Cui, D., Huang, J., Zhen, X., Li, J., Jiang, Y., & Pu, K. (2019). A semiconducting polymer nano-prodrug for hypoxia-activated photodynamic cancer therapy. Angewandte Chemie, 131(18), 5981-5985. doi:10.1002/ange.201814730

https://hdl.handle.net/10356/83296

https://doi.org/10.1002/ange.201814730

COMMUNICATION

Semiconducting Polymer Nano-prodrug for Hypoxia-activated Synergetic Photodynamic Cancer therapy

Dong Cui, Jiaguo Huang, Xu Zhen, Jingchao Li, Yuyan Jiang and Kanyi Pu*

Abstract: Photodynamic therapy (PDT) holds great promise for cancer therapy; however, its efficacy is often compromised by tumor hypoxia. We herein synthesize a semiconducting polymer nanoprodrug (SPNpd) that not only efficient generates singlet oxygen ($^1O_2$) under near-infrared (NIR) photoirradiation but also specifically activates its chemotherapeutic action in hypoxic tumor microenvironment. SPNpd is self-assembled from a amphiphilic polymer brush which comprises a light-responsive photodynamic backbone grafted with poly(ethylene glycol) (PEG) and conjugated with the chemodrug molecules via hypoxia-cleavable linkers. Such a well-defined and compact nanostructure of SPNpd (30 nm) enables preferable accumulation in the tumor of living mice. By virtue of these molecular advantages, SPNpd exerts synergistic photodynamic and chemo-therapy, and effectively inhibit tumor growth in xenograft tumor mouse model, which is not possible for its prodrug-free counterpart. This study thus represents the first hypoxia-activatable phototherapeutic polymeric prodrug system with a high potential for cancer therapy.

Phototherapy that utilizes photoirradiation to ablate malignant cells has emerged as a promising approach for cancer therapy.[1] As compared to conventional chemotherapy and radiotherapy, phototherapeutic modalities including photodynamic therapy (PDT) and photothermal therapy (PTT) has the advantages of non-invasiveness, minimal side effects, and relatively high therapeutic selectivity.[2] In particular, PDT capitalizes on photosensitizers to convert light energy into cytotoxic reactive oxygen species (ROS) to induce well-controlled regional cell apoptosis and tissue damage.[3] As a key component for PDT, photosensitizers have been continuously optimized for improved therapeutic efficacies. In addition to small-molecule dyes, many inorganic and organic nanomaterials have been exploited as photosensitizers, which include metallic nanoparticles,[4] gold nanoclusters,[5] quantum dots,[6] two-dimensional materials,[7] upconverting nanoparticles[8] and organic porphysomes.[9]

Despite the promise of PDT in cancer therapy, its oxygen reliance limits the therapeutic effect against tumor hypoxia. In fact, as a result of oxygen consumption and microvascular damage during PDT, PDT even increases the tumor hypoxia to a certain extent and further decreases its antitumor efficacy.[10] To overcome this issue, two strategies have been developed. One is to directly increase oxygenation in tumor by incorporation of oxygen-generating components such as perfluorocarbon and enzymes into photodynamic nanoparticles.[11] The other is to combine PDT with chemotherapy, which uses the hypoxia-responsive carrier to encapsulate both photosensitizers and chemodrugs into the nanoparticles.[12] Although chemophototherapy is an emerging treatment for solid tumors, [13] most of these chemophototheraputic agents are multicomponent systems, which suffer from the difficulty in quality control of nanoparticles preparation; moreover, they bear the risk of release/activation of chemodrug in normal tissues.

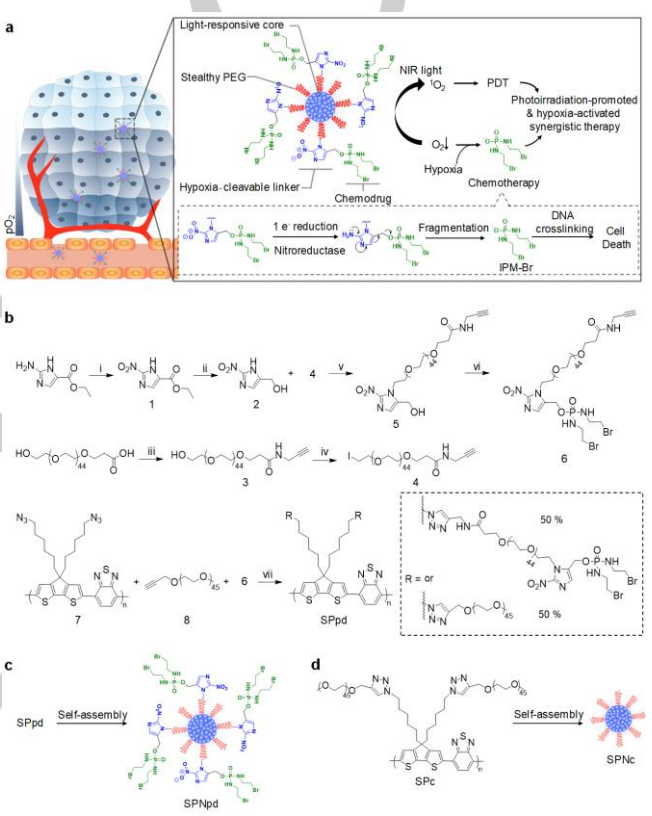

Figure 1. Molecular mechanism of SPNpd for synergistic cancer therapy. (a) Schematic illustration of SPNpd for hypoxia-activated synergistic photodynamic therapy and chemotherapy. (b) Synthetic route and preparation of SPNpd and the drug-free control nanoparticle (SPNc). Reagents and conditions: i) AcOH, $NaNO_2$, rt, 4 h. ii) $NaBH_4$, I_2, tetrahydrofuran, 40 ºC, 24 h. iii) Propargylamine, 1-Ethyl-3-(3-dimethylaminopropyl) carbodiimide hydrochloride, CH_2Cl_2, rt, 24 h. iv) PBr_3, CH_2Cl_2,, 0 ºC→rt, 12 h; NaI, acetone, 55 ºC, 48 h. v) $CsCO_3$, CH_3CN, 60 ºC, 48 h. vi) IPM-Br, PPh_3, DIAD, THF, 0 °C → rt, 6 h. vii) CuBr, N, N, N', N″ , N″ -pentamethyldiethylenetriamine, THF, 30 °C, 24 h. (c) and (d) Scheme of formation of SPNpd and SPNc

As a new category of organic phototheranostic agents, semiconducting polymer nanoparticles (SPNs) have gained growing attention due to their diversified optical properties and ideal biophysical features.[14] SPNs have been applied not only for molecular optical imaging including near-infrared (NIR) fluorescence,[15] chemiluminescence,[16] photoacoustic[17] and afterglow imaging,[18] but also for light control of biological activity including enzymatic activity,[19] protein ion channels,[20] and protein expression.[21] Moreover, structural modification of precursor polymers has led to SPN-based phototherapeutic

[*] D. Cui, Dr. J. Huang, Dr. X. Zhen, Dr. J. Li, Y. Jiang, Prof. K. Pu
School of Chemical and Biomedical Engineering
Nanyang Technological University
70 Nanyang Drive, Singapore 637457
E-mail: kypu@ntu.edu.sg

Supporting information for this article is given via a link at the end of the document.

agents able to convert photoenergy to heat or ROS for PTT or PDT.[22] For instance, we have recently synthesized a hybrid core-shell nanoparticle composed of manganese dioxide (MnO_2) nanosheets as the shell and SPN as the core to undergo O_2 evolution in tumor microenvironment for enhanced PDT.[23]

In this work, we synthesize a semiconducting polymer nano-prodrug (SPNpd) with a well-defined structure for hypoxia-activated synergistic cancer therapy. This nano-prodrug is assembled from an amphiphilic semiconducting brush polymer grafted with chemodrug side chains through hypoxia-cleavable linker. It has three key units (Figure 1a): the light-responsive photodynamic SPN core, hypoxia-cleavable linker and the chemotherapeutic drug, a bromoisophosphoramide mustard intermediate (IPM-Br). IPM-Br has been used for the treatment of a range of cancers, which is known to induce DNA crosslinking and cellular apoptosis.[24] Upon photoirradiation at 808 nm, SPNpd can generate singlet oxygen ($^1O_2$) for PDT; meanwhile, the tumor hypoxia in association with photoirradiation-depleted oxygen level specifically initiates the fragmentation and release of IPM-Br catalyzed by nitroreductase, leading to cell death. As such, SPNpd seamlessly integrates PDT with hypoxia-activated chemotherapy for synergistically amplified cancer therapy.

The drug-conjugated polymer (SPpd) and the drug-free control polymer (SPc) were synthesized via a graft-on approach (Figure 1b). To construct the drug-conjugated PEG (6), (2-nitro-1H-imidazol-5-yl) methanol (compound 2) was firstly synthesized *via* nitrification of ethyl 2-amino-1H-imidazole-5-carboxylate followed by ester reduction reaction. The iodide-PEG-alkyne (4) was synthesized via amidation of HO-PEG-carboxymethyl followed by halogen substitution reaction. The drug-conjugated PEG (6) was synthesized via substitution between 2 and 4, followed by phosphorylation. The ^{1}H NMR spectrum (Figure S5, Supporting Information) showed that the characteristic proton resonance peak of -NH-C*H*$_2$-CH$_2$-Br and -NH-CH$_2$-C*H*$_2$-Br in IPM-Br were found at 2.95 ppm and -O-C*H*$_2$-CH2-, -O-CH$_2$-C*H*$_2$- in PEG were found at 3.93-3.37 ppm, implying the correct structure of 6. The final product SPpd was synthesized via copper(I)-catalyzed alkyne-azide cycloaddition (CAAC) reaction of the azide-modified polymer (polymer 7), compound 6, and mPEG-alkyne (the molar ratio of 6 to mPEG-alkyne was 1). As shown in the ^{1}H NMR spectra of SPpd (Figure S6, Supporting Information), the characteristic proton resonance peaks of 7 were found at 8.12-7.63, 1.38 and 0.88 ppm. SPc was also synthesized via CAAC reaction of 7 and mPEG-alkyne. The gel permeation chromatography (GPC) data showed that the number-average molecular weights of SPpd and SPc were ~ 20000 with good polydispersity (PDI) (Table S1, Supporting Information).

Both SPpd and SPc assembled into the nanoparticles due to their amphiphilic nature in aqueous solution (termed as SPNpd and SPNc, respectively) (Figure 1c and 1d), forming the translucent solutions (Figure 2a). The transmission electron microscopy (TEM) showed both SPNpd and SPNc have uniform spherical morphology with an average diameter of ~ 30 nm (Figure 2b), nearly identical to the dynamic light scattering (DLS) (Figure 2c). In PBS (pH = 7.4), SPNpd and SPNc had the zeta potentials of -10.3 and -13.7 mV, respectively (Figure 2e). After storage in PBS for 20 days, no precipitation or obvious change in size was observed for both nanoparticles (Figure 2d). Both SPNs had similar absorption ranging from 450 to 900 nm with the maximum at 690 nm ((Figure 2f), and their fluorescence maximum was at 820 nm (Figure 2g). To investigate the photodynamic property, $^1O_2$ sensor green (SOSG) was used. Under photoirradiation at 808 nm for 4 mins, the fluorescence of SOSG at 528 nm increased by ~4.60-fold for SPNpd and SPNc (Figure 2f), proving that they had the identical photodynamic property under normoxic environment. The $^1O_2$ generation efficiencies (ΦΔ) of SPNpd (3.75%) and SPNc (3.73%) were ~18 times higher than indocyanine green (ICG) (ΦΔ = 0.2%). These data indicated that the conjugation of the hypoxic activated-prodrug had minimal influence on the optical and photodynamic properties of SPNpd.

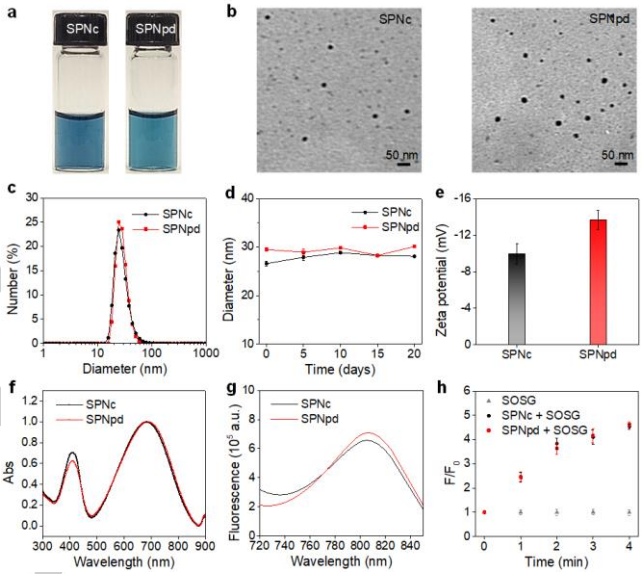

Figure 2. In vitro characterization. (a) Photos of nanoparticle solutions (30 μg mL^{-1}). (b) TEM images of SPNpd and SPNc. (c) DLS data of SPNpd and SPNc. (d) DLS data of SPNpd and SPNc as a function of incubation time in PBS (pH = 7.4). (e) ζ-Potentials of SPNpd and SPNc. (f) UV−vis absorption and (g) fluorescence spectra of SPNpd and SPNc. (h) Generation of $^1O_2$ determined by increased fluorescence intensity of SOSG in the absence or presence of SPNpd and SPNc (30 μg mL^{-1}) as a function of photoirradiation time (808 nm, 0.3 W cm^{-2}). Error bars represent the standard deviations of three separate measurements (n = 3).

To prove the hypoxia-induced prodrug activation of SPNpd, high-performance liquid chromatography (HPLC) analysis was used. SPNpd was first mixed with nitroreducase (NTR) after incubation with nicotinamide adenine dinucleotide (NADH) under anaerobic condition for 6 h (Figure 3a). The resulting solution was then analyzed by HPLC. An elution peak at 12.82 min corresponding to IPM-Br was observed in the HPLC trace of the resulting solution (Figure 3b), indicating that the NTR-induced activation of SPNpd and the subsequent release of IPM-Br. This phenomenon could be explained as following: the nitro groups of SPNpd were reduced to amino groups catalyzed by NTR followed by the release of IPM-Br under hypoxic environment (Figure 1a).

Confocal fluorescence imaging revealed that both SPNpd and SPNc had a similar cell uptake with the nearly same fluorescence intensity (Figure 3c), probably because of their similar sizes and surface zeta potentials. [3-(4,5-Dimethyl-thiazol-2-yl)-5-(3-

carboxymethoxyphenyl)-2-(4-sulfophenyl)-2H-tetrazolium] (MTS) was applied for cell viabilities tests. Under normoxic condition, without photoirradiation, both SPNpd and SPNc had negligible cytotoxicity against 4T1 cells even at a high concentration of 100 μg mL^{-1} (Figure 3d). Upon NIR photoirradiation at 808 nm, the cell viability of SPNc (45.7%) and SPNpd (43.7%) treated cells had no significant differences. This indicated that the prodrug was not activated and the conjugation of prodrug had no obviously impact on the PDT efficacy of SPNpd under the normoxic condition, which was consistent with SOSG assay results. However, under hypoxic condition without photoirradiation, the cell viability of SPNpd treated cells decreased to 34.1%, 2.5 times lower than that of SPNpd under normoxic condition (84.8%) (Figure 3e), indicating the prodrug activation. With NIR photoirradiation under hypoxic condition, the cell viability of SPNpd-treated cells further reduced to 8.3 %, 4.3 times lower than SPNc (35.7%). These data confirmed the chemotherapeutic ability of SPNpd was only activated under hypoxic condition and synergized with PDT for amplified therapeutic effect.

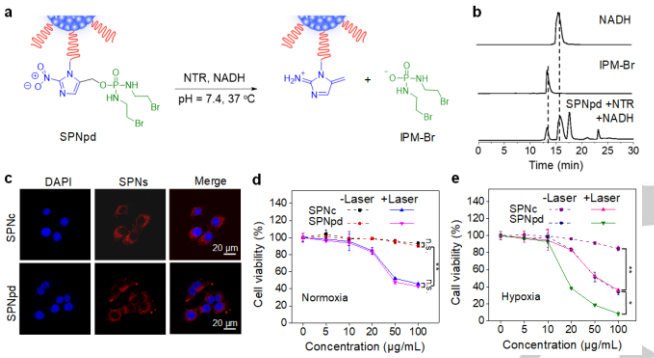

Figure 3. *In vitro* study of prodrug activation, cellulr uptake and cytotoxicity. (a) Scheme of prodrug activation and drug releasing study. (b) HPLC profiles of NADH (200 μM), IPM-Br (10 μg mL^{-1}) and the resulting solution of SPNpd after incubation with nicotinamide adenine dinucleotide (NADH) under anaerobic condition for 6 h. (c) Confocal fluorescence images of 4T1 cells incubation with SPNpd and SPNc (30 μg mL^{-1}) for 12 h. The blue fluorescence stands for the cell nuclei which were stained with 4,6-diamidino-2-phenylindole (DAPI). Cell viability of 4T1 cells after incubation with SPNc or SPNpd at various concentrations under normoxic (d) or hypoxic (e) environment, with or without photoirradiation (808 nm, 0.3 W cm^{-2}). Error bars represent the standard deviations of three separate measurements (n = 3). n.s. means no significance, *p < 0.05, **p < 0.01 and ***p < 0.001.

To identify the optimal in vivo phototherapeutic timepoint for SPNpd, NIR fluorescence imaging was conducted in the subcutaneous 4T1 xenograft tumor mouse model. After systemic administration of SPNpd or SPNc into the tumor-bearing living mice through tail vein, the NIR fluorescence images were longitudinally acquired (Figure 4a). The fluorescence of tumors gradually increased and reached maximum at 24 h post-injection for both SPNs (Figure 4b), indicating that both SPNs could passively accumulate in the tumor via the enhanced permeability and retention (EPR) effect. Additionally, ex vivo data showed that both SPNs had similar biodistribution (Figure S7, Supporting Information), and more importantly the fluorescence intensity of tumor was 1.5-fold higher than that of liver for both SPNs (Figure 4c), indicating the preferred accumulation at tumor site.

Because the tumors had the highest fluorescence intensities at 24 h post-injection of SPNc, or SPNpd, NIR photoirradiation was conducted at this time point for cancer phototherapy. Under NIR photoirradiation at 808 nm, the tumor temperatures for both SPNs-treated mice gradually increased (Figure 4d&4e); however, the maximum temperatures for both SPNs-treated mice were controlled below the apoptosis threshold temperature (43 °C) so that the photothermal effect was minimized.[25] To evaluate the *in vivo* therapeutic effect, the tumor sizes were monitored continuously for 15 days after treatment (Figure 4f). Without photoirradiation, the tumor for SPNc or SPNpd treated mice showed similar growth rate as that for saline-treated mice, indicating no therapeutic effect for both SPNs. This also reflected that despite the presence of the prodrug units in SPNpd, the prodrug was inactive probably because SPNpd was accumulated at the position of tumor where the hypoxia was not high enough. With photoirradiation, the tumor growth of SPNc-treated mice was only slow down; in contrast, the tumor growth of SPNpd-treated mice was effectively deterred. This proved that the solo PDT induced by the SPN core was unable to inhibit the tumor growth. However, as the oxygen in the hypoxic tumor microenvironment was further depleted by PDT process, SPNpd was activated and the toxic drug (IPM-Br) was released, leading to the synergetic PDT and chemotherapy for amplified antitumor efficacy.

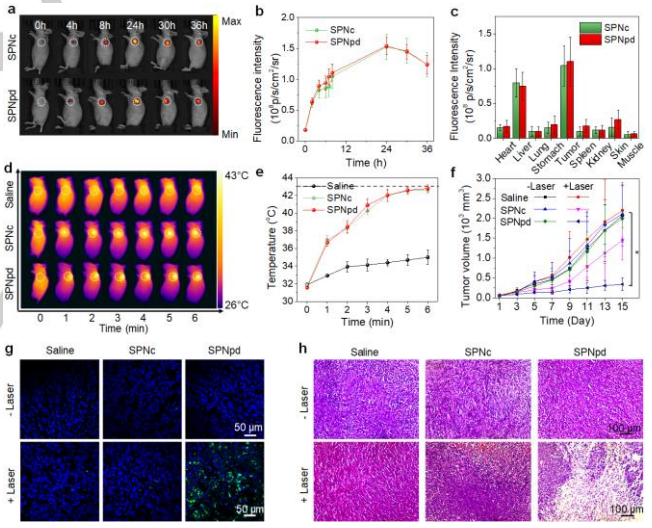

Figure 4. *In vivo* NIR fluorescence imaging and synergistic cancer therapy. (a) Representative NIR fluorescence images of 4T1 tumor-bearing living mice at different time points after intravenous injection of SPNpd,SPNc (400 μg mL^{-1}, 0.2 mL). NIR fluorescence images were acquired for 0.1 s at 840 ± 10 nm upon excitation at 675 ± 10 nm. The tumor site is marked by white circle. (b) Quantification of NIR fluorescence intensities of tumor as a function of post-injection time of SPNpd or SPNc. (c) Quantification of major organs of mice 36 h after systemic administration of SPNpd or SPNc. Error bars were based on standard error of mean (SEM) (n = 3). (d) IR thermal images of 4T1 tumor-bearing mice at 24 h post-injection of saline, SPNc, or SPNpd (400 μg mL^{-1}, 0.2 mL) after NIR photoirradiation at 808 nm (0.3 W cm^{-2}) for different amount of time. The tumor site is marked by white circle. (e) Mean tumor temperature during NIR photoirradiation at 24 h post-injection of saline, SPNc, or SPNpd (400 μg mL^{-1}, 0.2 mL) into 4T1 tumor-bearing mice. Error bars are based on standard error of mean (SEM) (n = 4). (f) Tumor growth curves for mice injected with saline, SPNc, or SPNpd (400 μg mL^{-1}, 0.2 mL) after photoirradiation for 6 min (*p < 0.05, n = 4). (g) Immunofluorescent staining of caspase-3 for the tumors of mice treated with saline, SPNc, or SPNpd (400 μg mL^{-1}, 0.2 mL) with

or without NIR photoirradiation. Green and blue fluorescence indicates caspase-3 and nucleus staining, respectively. The tumors for immunofluorescent staining of caspase-3 were collected after 15 days of treatment. (scale bars = 50 μm). (h) H&E staining of tumors from different treatment mice groups.

All mice groups had no significant weight loss for 15 days after treatment (Figure S8, Supporting Information) and no noticeable histopathological abnormalities were found in all major organs (Figure S9, Supporting Information), showing the good biosafety of both SPNs. Immunofluorescence caspase-3 staining revealed that without photoirradiation, no green fluorescence from the apoptotic cells was observed for both SPNs-treated mice. By contrast, with photoirradiation, stronger fluorescence from apoptotic cells was detected for the tumor tissues of SPNpd-treated mice as compared those with saline or SPNc treated mice. Similarly, hematoxylin and eosin (H&E) staining showed more necrotic cells for SPNpd-treated mice relative to SPNc-treated mice with photoirradiation, whereas other groups showed no obvious cell necrosis (Figure 4h). The histological analysis further verified the superior synergetic PDT and chemotherapy efficacy of SPNpd over the solo PDT of SPNc.

In summary, we have synthesized an organic photodynamic nano-prodrug (SPNpd) that can specifically release the chemodrug under photoirradiation-promoted hypoxia tumor microenvironment to exert synergetic PDT and chemotherapy. SPNpd possessed the photodynamic efficacy 18 times higher than ICG. Moreover, owing to its hypoxia-activated synergetic therapeutic effect, SPNpd showed 4.3-times higher anticancer efficacy as compared with its prodrug-free counterpart (SPNc) under NIR photoirradiation and hypoxic condition. After systemic administration, both SPNpd and SPNc effectively accumulated at the tumor of living mice due to their small sizes and stealthy PEG grafting. Without NIR photoirradiation, no obvious antitumor effect was observed for both SPNs, implying the inactivation of SPNpd. In contrast, photoirradiation effectively inhabited the tumor growth of SPNpd-treated mice, which was not possible for SPNc. Along with immunofluorescence staining and H&E staining, the *in vivo* data validated that SPNpd acted as a photoirradiation-promoted and hypoxia-responsive nanoprodrug for synergetic PDT and chemotherapy. To the best of our knowledge, SPNpd represents the first hypoxia-responsive phototherapeutic polymeric prodrug. In view of its high biosafety, preferable accumulation in tumor and NIR light response, such an organic phototherapeutic prodrug holds great promise for synergetic cancer therapy.

Acknowledgements

This work was supported by Nanyang Technological University (Start-Up grant: NTU-SUG: M4081627.120) and Singapore Ministry of Education Academic Research Fund Tier 1 (RG133/15 M4011559, 2017-T1-002-134-RG147/17) and Tier 2 (MOE2016-T2-1-098).

Keywords: photodynamic therapy • prodrug • polymer nanoparticles • fluorescence imaging • cancer therapy

[1] D. E. Dolmans, D. Fukumura, R. K. Jain, *Nat. Rev. Cancer* **2003**, *3*, 380-387.
[2] C. Liang, L. Xu, G. Song, Z. Liu, *Chem. Rev.* **2016**, *45*, 6250-6269.
[3] J. F. Lovell, T.W.B. Liu, J. Chen, G. Zheng, *Chem. Rev.* **2010**, *110*, 2839-2857.
[4] N. Kotagiri, G. P. Sudlow, W. J. Akers, S. Achilefu, *Nat. Nanotechnol.* **2015**, *10*, 370-379.
[5] C.-P. Liu, T.-H. Wu, C.-Y. Liu, K.-C. Chen, Y.-X. Chen, G.-S. Chen, S.-Y. Lin, *Small.* **2017**, *13*, 1700278.
[6] A. C. S. Samia, X. Chen, C. Burda, *J. Am. Chem. Soc.* **2003**, *125*, 15736-15737.
[7] a) J. Ge, M. Lan, B. Zhou, W. Liu, L. Guo, H. Wang, Q. Jia, G. Niu, X. Huang, H. Zhou, X. Meng, P. Wang, C.-S. Lee, W. Zhang, X. Han, *Nat. Commun.* **2014**, *5*, 4596; b) B. Tian, C. Wang, S. Zhang, L. Feng, Z. Liu, *ACS Nano* **2011**, *5*, 7000-7009.
[8] a) Y. Liu, Y. Liu, W. Bu, C. Cheng, C. Zuo, Q. Xiao, Y. Sun, D. Ni, C. Zhang, J. Liu, J. Shi, *Angew. Chem. Int. Ed.* **2015**, *54*, 8105-8109; *Angew. Chem.* **2015**, *127*, 8223-8227; b) J. Xu, L. Xu, C. Wang, R. Yang, Q. Zhuang, X. Han, Z. Dong, W. Zhu, R. Peng, Z. Liu, *ACS Nano* **2017**, *11*, 4463-4474.
[9] J. F. Lovell, C. S. Jin, E. Huynh, H. Jin, C. Kim, J. L. Rubinstein, W. C. W. Chan, W. Cao, L. V. Wang, G. Zheng, *Nat. Mater.* **2011**, *10*, 324-332.
[10] B. W, Henderson, V. H, Fingar, *Cancer Res.* **1987**, *47*, 3110-3114.
[11] a) Y. Cheng, H. Cheng, C. Jiang, X. Qiu, K. Wang, W. Huan, A. Yuan, J. Wu, Y. Hu, *Nat. Commun.* **2015**, *6*, 8785; b) H. Chen, J. Tian, W. He, Z. Guo, *J. Am. Chem. Soc.* **2015**, *137*, 1539-1547.
[12] C. Qian, J. Yu, Y. Chen, Q. Hu, X. Xiao, W. Sun, C. Wang, P. Feng, Q.-D. Shen, Z. Gu, *Adv. Mater.* **2016**, *28*, 3313-3320.
[13] D. Luo, K. A. Carter, D. Miranda, J. F. Lovell, *Adv. Sci.* **2017**, *4*, 1600106.
[14] a) C. Zhu, L. Liu, Q. Yang, F. Lv, S. Wang, *Chem Rev.* **2012**, *112*, 4687-4735; b) C. Wu, D. T. Chiu, *Angew. Chem., Int. Ed.* **2013**, *52*, 3086-3109; *Angew. Chem.* **2013**,*125*, 3164-3190; c) Y. Jiang, K. Pu. *Acc. Chem. Res.* **2018**, *51*, 1840-1849; d) J. Li, K. Pu. *Chem. Soc. Rev.* **2019**, 48, 38-71.
[15] G. Hong, Y. Zou, A. L. Antaris, S. Diao, D. Wu, K. Cheng, X. Zhang, C. Chen, B. Liu, Y. He, J. Z. Wu, J. Yuan, B. Zhang, Z. Tao, C. Fukunaga, H. Dai, *Nat. Commun.* **2014**, *5*, 4206.
[16] a) X. Zhen, C. Zhang, C. Xie, Q. Miao, K. L. Lim, K. Pu, *ACS Nano.* **2016**, *10*, 6400-6409; b) X. Zhen, Y. Tao, Z. An, P. Chen, C. Xu, R. Chen, W. Huang, K. Pu, *Adv. Mater.* **2017**, *29*, 1606665.
[17] a) K. Pu, A. J. Shuhendler, J. V. Jokerst, J. Mei, S. S. Gambhir, Z. Bao, J. Rao, *Nat Nanotechnol.* **2014**, *9*, 233-239; b) C. Xie, X. Zhen, Y. Lyu, K. Pu, *Adv. Mater.* **2017**, *29*, 1703693; c) Q. Miao, K. Pu, *Adv. Mater.* **2018**, *30*, 1801778.
[18] a) Q. Miao, C. Xie, X. Zhen, Y. Lyu, H. Duan, X. Liu, J. V. Jokerst, K. Pu, *Nat Biotechnol.* **2017**, *35*, 1102-1110. b) C. Xie, X. Zhen, Q. Miao, Y. Lyu, K. Pu, *Adv. Mater.* **2018**, *30*, 1801331
[19] J. Li, C. Xie, J. Huang, Y. Jiang, Q. Miao, K. Pu, *Angew. Chem., Int. Ed.* **2018**, *57*, 3995-3998; *Angew. Chem.* **2018**, *130*, 4059-4062.
[20] Y. Lyu, C. Xie, S. A. Chechetka, E. Miyako, K. Pu, *J. Am. Chem. Soc.* **2016**, *138*, 9049-9052.
[21] Y. Lyu, D. Cui, H. Sun, Y. Miao, H. Duan, K. Pu, *Angew. Chem., Int. Ed.* **2017**, *56*, 9155-9159; *Angew. Chem.* **2017**, *129*, 9283-9287.
[22] a) Y. Lyu, Y. Fang, Q. Miao, X. Zhen, D. Ding, K. Pu, *ACS Nano* **2016**, *10*, 4472-4481; b) Y. Lyu, J. Zeng, Y. Jiang, X. Zhen, T. Wang, S. Qiu, X. Lou, M. Gao, K. Pu, *ACS Nano* **2018**, *12*, 1801-1810. c) X. Zhen, C. Xie, K. Pu, *Angew. Chem., Int. Ed.* **2018**, *57*, 3938-3942; *Angew. Chem.* **2018**, *130*, 4002-4006; d) J. Li, X. Zhen, Y. Lyu, Y. Jiang, J. Huang, K. Pu. *ACS Nano* **2018**, 12, 8520-8530.
[23] a) H. Zhu, J. Li, X. Qi, P. Chen, K. Pu, *Nano Lett.* **2018**, *18*, 586-594; b) H. Zhu, Y. Fang, Q. Miao, X. Qi, D. Ding, P. Chen, K. Pu. *ACS Nano* **2017**, 11, 8998-9009.
[24] J. Duan, H. Jiao, J. Kaizerman, T. Stanton, J. W. Evans, L. Lan, G. Lorente, M. Banica, D. Jung, J. Wang, H. Ma, X. Li, Z. Yang, R. M. Hoffman, W. S. Ammons, C. P. Hart, M. Matteucci. J. Med. Chem., 2008, 51, 2412-2420.
[25] C. S. Jin, J. F. Lovell, J. Chen, G. Zheng, *ACS Nano* **2013**, *7*, 2541-2550.

COMMUNICATION

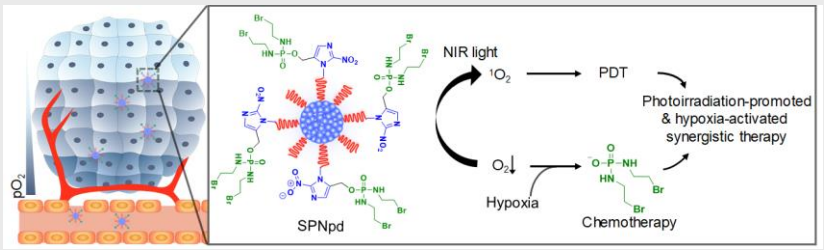

A semiconducting polymer nano-prodrug is synthesized to not only efficiently generate singlet oxygen under near-infrared (NIR) photoirradiation but also specifically activate its chemotherapeutic action in hypoxic tumor, affording synergistic photodynamic cancer therapy

*Dong Cui, Jiaguo Huang, Xu Zhen, Jingchao Li, Yuyan Jiang and Kanyi Pu**

Page No.1– Page No.5

Title: Semiconducting Polymer Nano-prodrug for Hypoxia-activated Synergetic Photodynamic Cancer therapy

[a] Title(s), Initial(s), Surname(s) of Author(s) including Corres
Author(s)
Department